Electronic Supplementary Material (ESI) for Lab on a Chip.

Electronic Supplementary Information

Integrated microfluidic platform with electrohydrodynamic focusing and carbon-nanotubes-based field-effect transistor immunosensor for continuous, selective, and label-free quantification of bacteria

Chang-Ho Han[a] and Jaesung Jang[a, b, †]

[a] Department of Mechanical Engineering, Ulsan National Institute of Science and Technology (UNIST), Ulsan 44919, Republic of Korea

[b] Department of Biomedical Engineering, UNIST, Ulsan 44919, Republic of Korea

[†]Correspondence should be addressed to jjang@unist.ac.kr; Tel: +82-52-217-2323; Fax: +82-52-217-2449

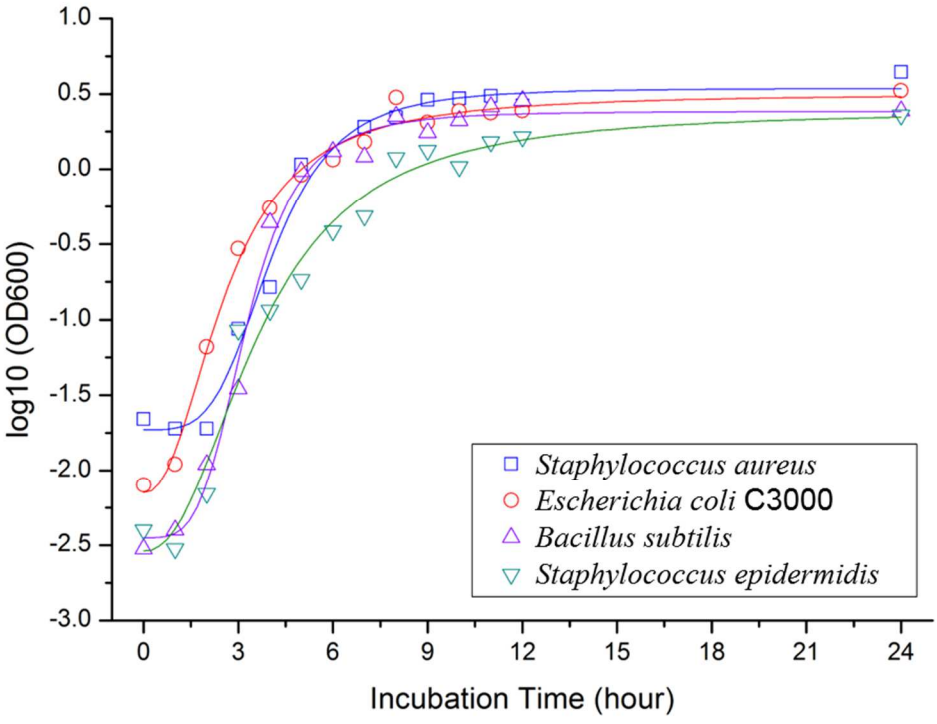

Figure S-1. Bacterial growth curves measured for the present study.

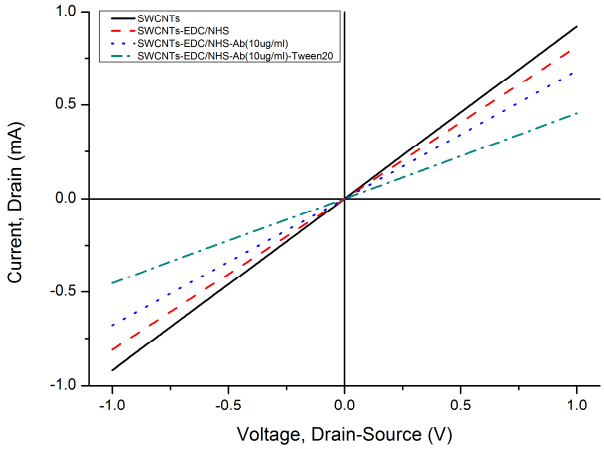

Figure S-2. *I-V* graphs for the detection electrodes with SWCNT channels modified with EDC/NHS, *S. aureus* antibody, and Tween 20.

Optimization process for EHD focusing

Alternating current (AC) frequencies and electric potentials were experimentally determined for electrohydrodynamic (EHD) focusing. Four parameters were investigated in the bead capture experiments, namely electro-osmosis (EO) frequency, EO electric potential, negative dielectrophoresis (nDEP) frequency, and nDEP electric potential. The number of captured beads (i.e., 380-nm-diameter polystyrene beads) was compared with the DEP fixed at the concentration electrodes, where one parameter among the aforementioned four parameters was varied while the other three were fixed. Figure S-3a shows the number of captured beads with varying EO frequency, showing that the peak value was 5.4 kHz. The maximal capture occurred at an EO potential of 1.25 Vpp. A larger convection speed could be induced when the EO potential was higher, but the risk of particle loss by inertial impaction could also increase (Fig. S-3b). A frequency of 3 MHz was deemed best for the nDEP frequency (Fig. S-3c). Although stronger nDEP forces were generated with this higher frequency in the megahertz regime, the superimposed signals were unstable when the nDEP frequency exceeded 3 MHz owing to the lab-made voltage adder limitations. Figure S-3d shows that the nDEP electric

potential in this case was determined as 10 Vpp, which was the maximal output voltage from the function generator.

For bacterial detection experiments, a pair of sinusoidal signals were used for EHD focusing. Only two parameters were investigated, i.e., EHD frequency and EHD electric potential, and one parameter was varied while the other was fixed. Then, the relative electrical conductance change (RCC) between the detection electrodes were compared. Here, the DEP (8 MHz, 10 Vpp) was applied to the concentration electrodes. Figure S-3e shows the stabilized relative electrical conductance change (SRC) was the highest at 9 kHz. The SRC was also the highest at an EHD potential of 1.5 Vpp when the frequency was fixed at 9 kHz (Fig. S-3f).

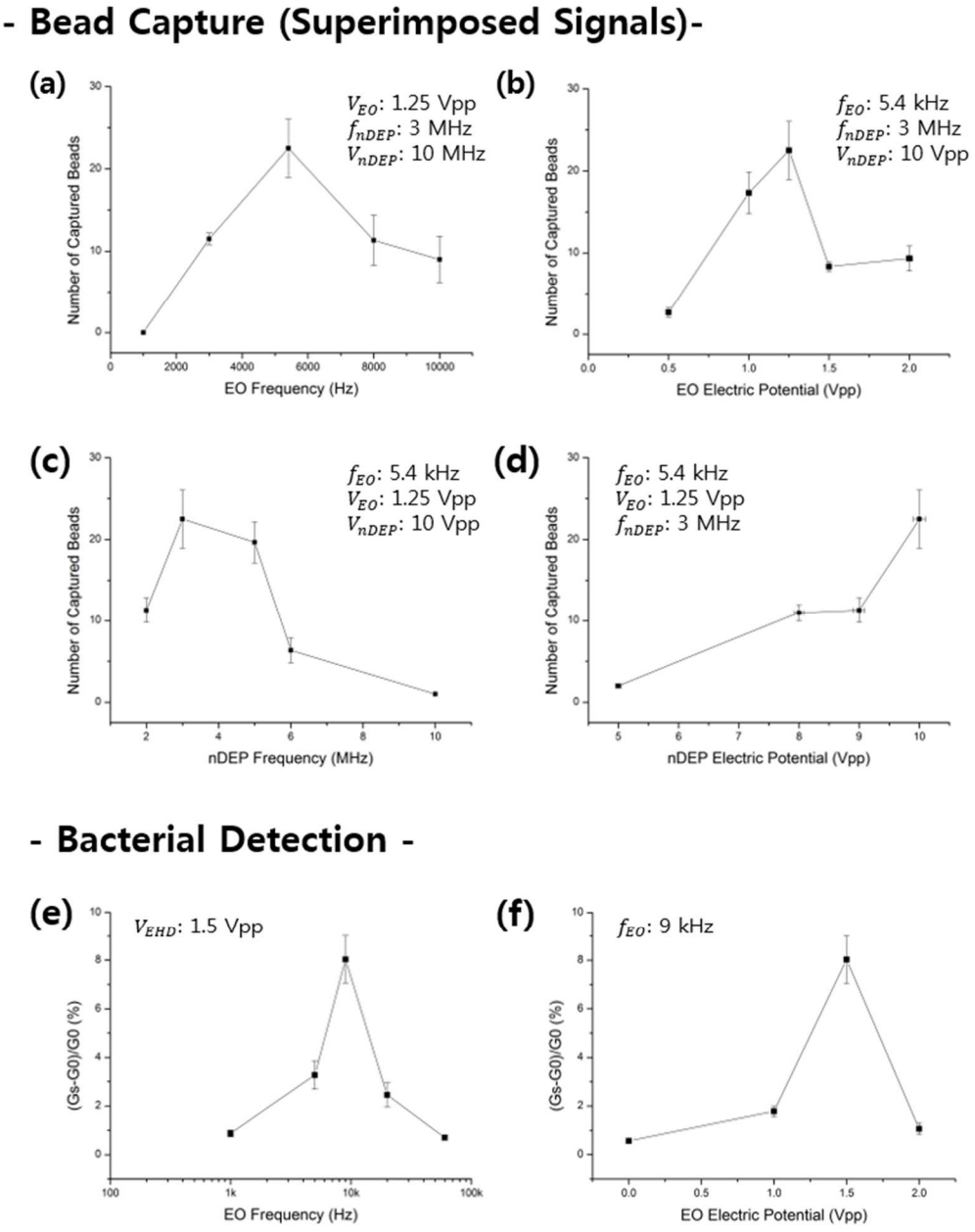

Figure S-3. Optimization process of the frequencies and electric potentials for EHD focusing. Among the four electrical components of the superimposed signals for bead capture, one parameter, namely **(a)** EO frequency, **(b)** EO electric potential, **(c)** negative DEP (nDEP) frequency, and **(d)** nDEP electric potential, was varied while the other three parameters were fixed. Between the two components of the sinusoidal signals for bacterial detection, one parameter, namely **(e)** EO frequency or **(f)** EO electric potential, was varied while the other parameter was fixed.

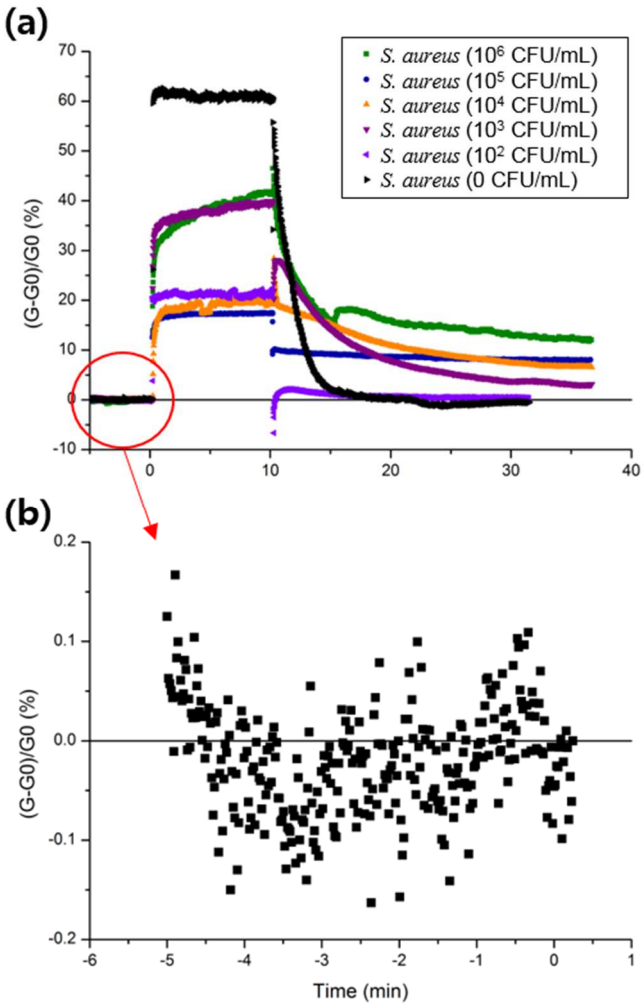

Figure S-4. (a) Figure 4a; **(b)** example showing electrical conductance variations with time.

PDMS microchannel fabrication

Master molds were fabricated on a 6-inch silicon substrate for the polydimethylsiloxane (PDMS) microchannels with channel mold width/height of 200 μm/49 μm by conventional photolithography with spin-coated negative tone SU-8 2050 (MicroChem Corp., USA) at 3000 rpm. The molds were silanized (trichloro(1H,1H,2H,2H-perfluoro-octyl)silane; 98% purity; 130672, Sigma-Aldrich, USA) for 1 h under a slight vacuum to peel the PDMS microchannels off easily during replica molding. A PDMS mixture (Sylgard® 184; Dow Corning Corp., USA) was gently poured on the prepared molds, while avoiding air bubbles, and cured at 70 °C for 2

h in a chamber[1].

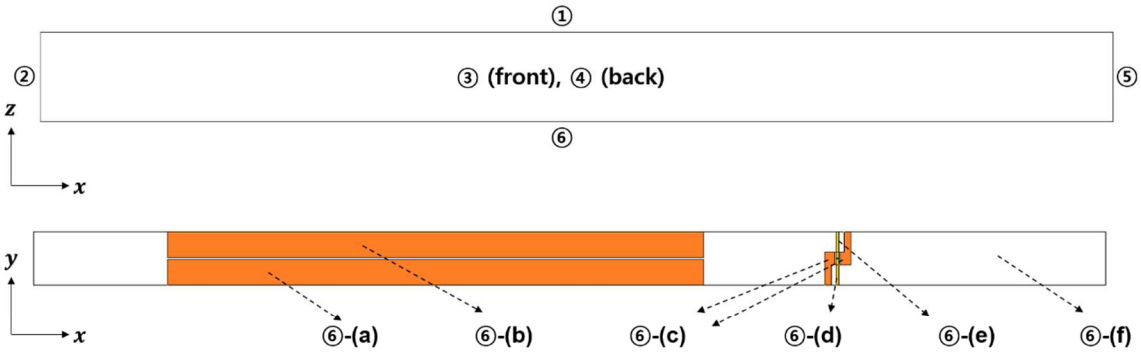

①,③,④,⑥-**(f)**:
$\frac{\partial \varphi}{\partial n} = 0$ (electric field), $\overline{u} = 0$ (flow field)
②:
$\frac{\partial \varphi}{\partial n} = 0$ (electric field), $\overline{u} = U_{ave}$ (flow field)
⑤:
$\frac{\partial \varphi}{\partial n} = 0$ (electric field), $p = 0$ (flow field)

⑥-**(a)**: $\varphi = \frac{V_{pp,EO}}{2}\sin\omega_{EO}t + \frac{V_{pp,nDEP}}{2}\sin\omega_{nDEP}t$ (electric field), $\overline{u} = \langle U_{EO}\rangle\hat{j}$ (flow field)
⑥-**(b)**: $\varphi = \frac{V_{pp,EO}}{2}\sin(\omega_{EO}t + \pi) + \frac{V_{pp,nDEP}}{2}\sin(\omega_{nDEP}t + \pi)$ (electric field), $\overline{u} = \langle U_{EO}\rangle\hat{j}$ (flow field)
⑥-**(c)**: $\frac{\partial \varphi}{\partial n} = 0$ (electric field), $\overline{u} = 0$ (flow field)
⑥-**(d)**: $\frac{\partial \varphi}{\partial n} = \frac{V_{pp,pDEP}}{2}\sin\omega_{pDEP}t$ (electric field), $\overline{u} = 0$ (flow field)
⑥-**(e)**: $\frac{\partial \varphi}{\partial n} = \frac{V_{pp,pDEP}}{2}\sin(\omega_{pDEP}t + \pi)$ (electric field), $\overline{u} = 0$ (flow field)

Figure S-5. Boundary conditions for the 3D Comsol simulations shown in Figs. 3c-d.

3D multiphysics simulations using COMSOL

3D simulations were conducted using the commercial software COMSOL Multiphysics® 4.3 to verify EHD focusing. A 4 mm long (x-), 200 μm wide (y-), and 49 μm high (z-) microchannel was designed with different electrode patterns on the bottom surface. All the boundary conditions used for the electric and flow fields are shown in Fig. S-5. The Laplace equation $\nabla^2\varphi = 0$ was first solved to find the quasi-static electric field, where φ is electric potential. The conjugate gradient method was used as an iterative solver for φ along the entire domain. The electric field vector fields were obtained from $\overline{E} = -\underline{\nabla}\varphi$. The governing equations for the flow fields were $\underline{\nabla} \cdot \overline{u} = 0$ and $\underline{\nabla} \cdot \left[-pI + \mu\left(\underline{\nabla}\overline{u} + \left(\underline{\nabla}\overline{u}\right)^{\mathrm{T}}\right)\right] = 0$, where $\overline{u}$ is the flow velocity vector, p is static pressure, and μ is the dynamic viscosity of the fluid. The EO slip flow (boundary conditions ⑥-(a) and ⑥-(b) in Fig. S-5) at the

focusing electrodes is expressed as $\langle U_{EO} \rangle = \frac{\Lambda \varepsilon_m {\varphi_0}^2 \Omega^2}{8\mu y(1+\Omega^2)^2}$, where $\Lambda = \frac{C_S}{C_S + C_D} \cong 0.5$ (C_S and C_D are Stern and diffuse layer capacitances, respectively)[2], ε_m is the electrical permeability of the medium (fluid), φ_0 is the initial potential, and Ω is a non-dimensional frequency defined as $\Omega = \frac{\Lambda \pi \varepsilon_m \omega}{2\sigma_m \lambda_D}$ with angular frequency ω, electrical conductivity of medium σ_m, and Debye length λ_D. Here, the y coordinate is equal to zero at the center of the focusing electrode gap. The Newton–Raphson algorithm was employed along with an iterative solver using the generalized minimum residual method; hence, the $\overline{u}$ and p fields were obtained along the volumetric domain.

Particle tracing was conducted for the bead using the Lagrangian discrete phase model equation $m_p \frac{d^2 \overline{x}_p}{dt^2} = \overline{F}_{drag} + \overline{F}_{gravity} + \overline{F}_{buoyancy} + \overline{F}_{DEP} = -3\pi\mu d_p \left(\frac{d\overline{x}_p}{dt} - \overline{u} \right) + m_p \frac{\rho_p - \rho}{\rho_p} \overline{g} + \frac{\pi}{4} {d_p}^3 \varepsilon_m Re(K) \underline{\nabla} \left| \overline{E} \right|^2$, where m_p is the particle mass, $\overline{x}_p$ is the position vector of the particle, d_p is the particle diameter, ρ_p is the particle density, $\overline{g}$ is the gravity vector, ε_m is the electrical permittivity of the medium, and $Re(K)$ is the real part of the Clausius–Mossotti factor. Here, the beads were 380-nm-diameter spheres, with ρ_p of 1050 kg/m^3. Predetermined $\overline{u}$ and $\overline{E}$ values were used for particle tracing, and a transient implicit-solver-generalized alpha was used with automatically chosen time steps. A total of 114 (19×6) particles were thus uniformly distributed at the inlet, and their position vectors were calculated with time. All the solutions numerically converged when the mesh exceeded 789,653 elements, and the 4th, 2nd, and 1st order elements were used for the electric potential, flow velocity, and pressure, respectively (with 4, 10, 20, and 35 nodes per tetrahedral element for the 1st, 2nd, 3rd, and 4th order elements respectively). The trajectories of the beads (Fig. 3c) were then obtained with zero electric potentials at the concentration electrodes.

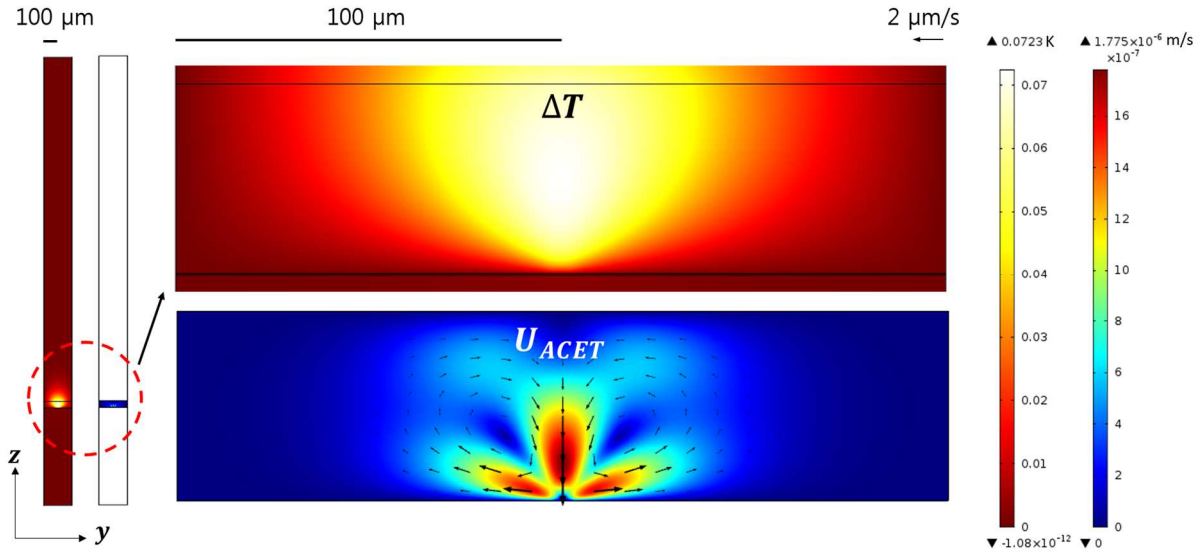

Figure S-6. Computed temperature rises and electrothermal velocity magnitudes in 0.01× PBS (10 Vpp, 8 MHz) around the concentration electrodes.

2D multiphysics simulations using COMSOL for electrothermal flow effect

2D simulations were conducted using the same software to estimate the AC electrothermal effects in the experiments. A cross-sectional (y-z plane) domain was set around the concentration electrodes (5-μm-gap) considering silicon substrate (675-μm-thick), SiO_2 layer (300-μm-thick), Si_3N_4 layer (300-μm-thick), 0.01× phosphate buffered saline (PBS; 49-μm-thick), and PDMS (2.4-mm-thick). Electrical governing equation $\nabla^2\varphi = 0$ was solved for the domain with boundary conditions of $\frac{\partial\varphi}{\partial n}$ at all outer boundaries, and $\varphi = \frac{V_{pp,pDEP}}{2}\sin\omega_{pDEP}t$ and $\varphi = -\frac{V_{pp,pDEP}}{2}\sin\omega_{pDEP}t$ at each concentration electrodes, where $V_{pp,pDEP}$ and ω_{pDEP} is the peak-to-peak voltage and angular frequency of AC signal for positive DEP, respectively. Thermal governing equation of $k\nabla^2 T + \frac{\sigma_m}{2}\left|\overline{E}\right|^2 = 0$ was solved for all domain with boundary conditions of $T = 23$ ℃ at the outer boundaries, where k is thermal conductivity and T is temperature[3,4]. Flow governing equations of $\underline{\nabla}\cdot\overline{u} = 0$ and $\underline{\nabla}\cdot\left[-pI + \mu\left(\underline{\nabla}\overline{u} + \left(\underline{\nabla}\overline{u}\right)^{\mathrm{T}}\right)\right] + \overline{F}_{ACET} + \overline{F}_{bouyancy} = 0$ was solved for 0.01× PBS (0.02 S/m)

domain only, with the boundary conditions of $\overline{u} = 0$. Here, $\overline{F}_{ACET} = \frac{\varepsilon_m}{2}\left[(c_\varepsilon - c_\sigma)\frac{\underline{\nabla}T\cdot\overline{E}}{1+(\omega_{pDEP}\varepsilon_m/\sigma_m)}\overline{E} - \frac{1}{2}c_\varepsilon\underline{\nabla}T\left|\overline{E}\right|^2\right]$ and $\overline{F}_{bouyancy} = -\rho_m(T - 23\ ℃)\beta\overline{g}$, where $c_\varepsilon \cong -0.004\ ℃^{-1}$, $c_\sigma \cong 0.02\ ℃^{-1}$, ρ_m is a density of media, $\beta \cong 0.001\ ℃^{-1}$, and $\overline{g}$ is gravity vector[3,4]. As results of calculations, the maximal possible temperature rise and flow velocity was 0.07 ℃ and 1.78 μm/s, respectively. The maximum temperature rises were calculated to be 0.68 ℃ and 6.24 ℃ in 0.1× PBS (0.186 S/m) and 1× PBS (1.59 S/m), respectively.

Table S-1. Determination of relative standard deviation (RSD).

S. aureus (10^4 CFU/mL) in 0.01x PBS	1	2	3	4	Mean value	Standard deviation (SD)	Relative standard deviation* (RSD; n=4)
	6.60	8.04	6.50	7.25	7.10	0.71	10.02%
*Relative standard deviation (RSD) = (SD/Mean)							

References

[1] C.-H. Han, H. W. Ha and J. Jang, *Lab Chip*, 2019, **19**, 1772-1782.
[2] M. Z. Bazant, M. S. Kilic, B. D. Storey and A. Ajdari, *Adv. Colloid Interfac.*, 2009, **152**, 48-88.
[3] N. G. Green, A. Ramos, A. Gonzalez, A. Castellanos and H. Morgan, *J. Electrostat.,* 2001, **53**, 71-87.
[4] S. Loire, P. Kauffmann, I. Mezic and C. D. Meinhart, *J. Phys. D: Appl. Phys.,* 2012, **45**, 185301.